J BONE ONCOL 43 (2023) 100510

Contents lists available at ScienceDirect

Journal of Bone Oncology

journal homepage: www.elsevier.com/locate/jbo

Research Paper

Evaluation of pain related behaviors and disease related outcomes in an immunocompetent mouse model of prostate cancer induced bone pain

Juan Miguel Jimenez-Andrade [c], Martha B. Ramírez-Rosas [c], Sun Hee Park [b], Renee Parker [a], Matthew R. Eber [b], Rebecca Cain [a], Mary Newland [a], Fang-Chi Hsu [d], Carol A. Kittel [d], Thomas J. Martin [a], Enriqueta Muñoz-Islas [c], Yusuke Shiozawa [b,*], Christopher M. Peters [a,*]

[a] Department of Anesthesiology, Wake Forest School of Medicine, Winston-Salem, NC, 27157, USA
[b] Department of Cancer Biology and Comprehensive Cancer Center, Wake Forest School of Medicine, Winston-Salem, NC, 27157, USA
[c] Universidad Autónoma de Tamaulipas, Campus Reynosa Aztlán, Reynosa, Tamaulipas, 88700 Mexico
[d] Department of Biostatistics and Data Science, Wake Forest School of Medicine, Winston-Salem, NC, 27157, USA

HIGHLIGHTS

- Immunocompetent C57BL/6 mouse models of prostate cancer induced bone pain are needed.
- RM1 prostate cancer injected into the femur produced mixed lytic and sclerotic lesions.
- Intra-femoral RM1 prostate cancer (PCa) induced progressive hindlimb guarding and impaired running wheel performance in mice.
- Intra-femoral RM1 PCa induced neurochemical changes in the dorsal root ganglia and spinal cord indicative of nerve injury, inflammation and central sensitization.

ARTICLE INFO

Keywords:
Bone metastasis
Oncology
Malignant bone pain
Nociceptor

ABSTRACT

Cancer-induced bone pain (CIBP) is the most common and devastating symptom of bone metastatic cancer that substantially disrupts patients' quality of life. Currently, there are few effective analgesic treatments for CIBP other than opioids which come with severe side effects. In order to better understand the factors and mechanisms responsible for CIBP it is essential to have clinically relevant animal models that mirror pain-related symptoms and disease progression observed in patients with bone metastatic cancer.

In the current study, we characterize a syngeneic mouse model of prostate cancer induced bone pain. We transfected a prostate cancer cell line (RM1) with green fluorescent protein (GFP) and luciferase reporters in order to visualize tumor growth longitudinally *in vivo* and to assess the relationship between sensory neurons and tumor cells within the bone microenvironment. Following intra-femoral injection of the RM1 prostate cancer cell line into male C57BL/6 mice, we observed a progressive increase in spontaneous guarding of the inoculated limb between 12 and 21 days post inoculation in tumor bearing compared to sham operated mice. Daily running wheel performance was evaluated as a measure of functional impairment and potentially movement evoked pain. We observed a progressive reduction in the distance traveled and percentage of time at optimal velocity between 12 and 21 days post inoculation in tumor bearing compared to sham operated mice. We utilized histological, radiographic and μCT analysis to examine tumor induced bone remodeling and observed osteolytic lesions as well as extra-periosteal aberrant bone formation in the tumor bearing femur, similar to clinical findings in patients with bone metastatic prostate cancer. Within the tumor bearing femur, we observed reorganization of blood vessels, macrophage and nerve fibers within the intramedullary space and periosteum adjacent to tumor cells. Tumor bearing mice displayed significant increases in the injury marker ATF3 and upregulation of the neuropeptides SP and CGRP in the ipsilateral DRG as well as increased measures of central sensitization and glial activation in the ipsilateral spinal cord. This immunocompetent mouse model will be useful when combined with cell type selective transgenic mice to examine tumor, immune cell and sensory neuron interactions in the bone

* Corresponding authors at: Department of Anesthesiology, Wake Forest School of Medicine, Medical Center Boulevard, Winston-Salem, North Carolina, 27157, USA (C.M. Peters); Department of Cancer Biology, Wake Forest School of Medicine, Medical Center Boulevard, Winston-Salem, North Carolina 27157, USA. (Y. Shiozawa).

E-mail addresses: yshiozawa@wakehealth.edu (Y. Shiozawa), chrpeter@wakehealth.edu (C.M. Peters).

https://doi.org/10.1016/j.jbo.2023.100510
Received 28 August 2023; Received in revised form 25 October 2023; Accepted 27 October 2023
Available online 30 October 2023

microenvironment and their role in pain and disease progression associated with bone metastatic prostate cancer.

1. Introduction

Prostate cancer is one of the most prevalent types of cancer in men. During advanced stages of the disease skeletal metastasis is common, occurring in 80–90 % of patients resulting in aberrant bone remodeling, skeletal instability and severe debilitating pain that substantially impairs normal activity and disrupts a patient's quality of life [1]. Cancer induced bone pain (CIBP) consists of both ongoing and movement related pain. Ongoing pain is typically dull in character, persistent, and progressive - getting worse as the tumor grows within the bone. Breakthrough pain is also a common symptom evident as a transient exacerbation of pain often associated with movement but can occur spontaneously that is resistant to common opioid analgesics [1,2]. Currently, the most effective analgesic treatments for CIBP are opioids, however they come with severe side effects and often lead to abuse.

CIBP is a complex pain state that is distinct from other types of chronic pain including inflammatory and neuropathic pain [3,4]. Bone is densely innervated [5,6] and bone cancer pain arises from a complex interaction between sensory neurons, tumor, stromal, and immune cells [5,6] within the bone microenvironment [7]. Preclinical studies demonstrate that CIBP is initially driven by several tumor derived factors including glutamate, nerve growth factor (NGF), interleukin-6 (IL-6), and endothelin-1 (ET-1) [8–11], which sensitize sensory neurons within the bone microenvironment. Secondly, a highly acidic environment is produced within the bone resulting from tumor induced osteoclast activation and enhanced bone resorption [12,13] as well as increased release of protons due to tumor induced hypoxia and tissue injury [2]. Increased release of protons and local acidosis leads to activation and sensitization of several acid sensing ion channels including the transient receptor potential vanilloid 1 (TRPV1) and acid sensing ion channels (ASIC3) which have been shown to contribute to CIBP [12–15]. Third, there is evidence of tumor induced injury and damage to the distal processes of sensory nerve fibers within bone at the leading edge of the tumor [16,17] suggesting a neuropathic component and analgesics effective for neuropathic conditions have shown some efficacy in preclinical models [17,18]. Finally, a profound pathological sprouting of sensory neurons has also been observed in several preclinical models of bone cancer pain particularly at later stages [19–21], whose blockade with therapies including anti-nerve growth factor or anti-netrin-1 antibodies reduce associated ongoing and movement evoked bone cancer pain [22,23].

While significant progress has been made regarding our understanding of mechanisms of bone cancer pain, it should be highlighted that most of this knowledge has been obtained from clinical studies on how to best manage pain in cancer patients and/or from sarcoma or breast cancer bone pain models in rodents [19,24,25,26,27]. The mechanisms that generate bone cancer pain due to metastatic prostate cancer may, in part, be different from sarcoma or breast cancer as metastatic prostate cancer produces simultaneously bone destruction and formation, which is quite distinct from that observed in tumors such as sarcoma or breast, where bone destruction predominates [27]. Furthermore, there still is a lot that is not known about the cellular interactions that drive different types of bone cancer pain and the contribution of discrete immune cells and subpopulations of neurons to pain and disease progression. It is worth mentioning that most of the research on prostate cancer induced bone pain comes from xenograft models in which the immune system is compromised [21,28–30] and may not accurately recapitulate important immune signaling and neuroimmune interactions present clinically. It has been established in prior studies both innate and adaptive immune cells play an essential role in the development and maintenance of chronic pain as well as in cancer disease progression [31,32]. Additionally, the few studies that have utilized allograft or syngeneic prostate bone cancer models to study pain have focused mostly on evaluating mechanical and thermal hypersensitivity referred to the tumor bearing paw [33–35] rather than measures of spontaneous or movement evoked pain, which may better mirror the behavioral symptoms observed in patients with metastatic prostate cancer.

In the current study, we refine an immunocompetent mouse model of prostate cancer induced bone pain involving orthotopic injection of the syngeneic RM1 cell line into the femur of C57BL/6 mice. We evaluated longitudinally the progression of spontaneous guarding behaviors as well as developed novel methods for evaluation of alterations in limb use with daily running wheel assessment. We also longitudinally assessed tumor growth, tumor induced bone remodeling and confirmed key neurochemical changes in the dorsal root ganglia and spinal cord of tumor bearing mice associated with CIBP. Lastly, we qualitatively examined the distribution of nerve fibers, macrophage and vasculature in the tumor bearing bone at early and late time points following tumor inoculation.

2. Methods

2.1. Animals

Experiments were performed using 51 male C57BL/6 mice (8 weeks old, Jackson Laboratories, Bar Harbor, ME, USA) weighing between 20 and 33 g. Mice were housed in accordance with NIH guidelines and conformed to the Wake Forest University Guidelines on the ethical use of animals, and studies were performed under Animal Care and Use Committee (Protocol A18-026, Winston-Salem, North Carolina) approval. Animals were housed under a 12-hour light–dark cycle, with food and water *ad libitum*.

2.2. Cell culture and injection of tumor cells

Prostate cancer induced bone pain model involved injection of RM-1 syngeneic prostate cancer cells (1 x10^3 cells/5μl) or sterile Hank's buffered saline as a sham control into the intramedullary space of the right femur of 8-week-old male mice. The parental RM-1 cell line [36] was a kind gift from Dr. Timothy Thompson (M. D. Anderson Cancer Center, Houston, TX). The RM1 carcinoma cell line was developed by retroviral transduction of cells to express the oncogenes Ras and Myc and implantation into urogenital sinus mouse prostate reconstitution model and is described as an admixture of luminal and epithelial cell carcinoma that is androgen dependent [36,37]. RM-1 cells were cultured in Dulbecco's Modified Eagle's medium (DMEM) (Fisher Scientific Gibco 11–995-073) supplemented with 10 % (V/V) fetal bovine serum (FBS) (Gibco 26–140-079), 1 % penicillin–streptomycin (10,000U/mL, Gibco 15–140-163), and 1 % L-Glutamine (200 mM, Gibco 25–030-164). Prior to injection, the parental RM-1 cell line was virally transfected with pGreenFire 1.0-mCMV lentivirus expressing green fluorescent protein (GFP) and firefly luciferase which allowed for flow cytometry-based cell sorting prior to inoculation (top 10 % of the GFP positive cells were sorted) and longitudinal *in vivo* bioluminescence imaging, respectively. The pGreenFire 1.0-mCMV lentivirus aliquots were purchased from the University of Michigan viral vector core. Accurate needle placement was confirmed radiographically prior to injection of cancer cells and the injection site was sealed with bone cement to delay spread of cancer cells to adjacent soft tissue.

2.3. Measures of bone remodeling

Mice were x-rayed every week using a digital cabinet Faxitron Bioptics MultiFocus X-ray system. To quantify the extent of bone destruction, a 5-point scale was used by an observer blind to condition as follows: 0, normal bone with no signs of destruction; 1, small pits (1–3 in number) of bone destruction; 2, increased pitted appearance (4–6 in number) and loss of medullary bone; 3, loss of medullary bone and erosion of cortical bone; 4, full thickness unicortical bone loss and 5, full thickness bicortical bone loss and displaced skeletal fracture similar to previous studies [38,39].

2.4. μCT analysis

A separate cohort of sham-operated (n = 8) and tumor-injected mice (n = 8) underwent μCT analysis 21 days post inoculation. Mice were deeply anesthetized using isoflurane, the thorax was opened, and 0.1 M phosphate-buffered saline (PBS, pH 7.4) followed by fixative (4 % paraformaldehyde in 0.1 M PBS, pH 7.4) was perfused through the left ventricle. Hindlimbs were collected postfixed for 24 h and washed several times in ice cold PBS prior to analysis. Micro-CT images of tibiofemoral knee joints were analyzed using a desktop micro-CT system (Skyscan 1272; Bruker, Brussels, Belgium). At the end of the experiment, mouse hindlimbs were removed and stored at a temperature of –20 °C in 0.1 M PBS (pH 7.4) until their analysis. The scanning process was conducted at a voxel size of 10 μm, an X-ray power of 60 kVp and 166 μA with an integration time of 627 ms, according to the guidelines for micro-CT analysis of rodent bone structure [40]. All the scanner images were reconstructed using NRecon Software (Bruker). The region of interest was bordered laterally by the cortex in a 2 mm band in the metaphysis, starting 0.5 mm from the growth plate. A hydroxyapatite calibration phantom was used to calibrate bone density values (250 and 750 mg/cm3). Trabecular bone volume rate (BV/TV), trabecular thickness (Tb.Th), trabecular number (Tb. N), trabecular separation (Tb. Sp.), degree of anisotropy and trabecular bone mineral density (BMD) were determined using CT analyzer software (Bruker). The acquisition settings for cortical analysis in the diaphyseal femur were the same as in the metaphyseal region. To calculate the morphologic cortical parameters, a region of interest was chosen inside the diaphyseal femur, selecting a band of 1 mm, starting 4 mm and extending distally from the growth plate. Cortical bone analyses were performed in the CT Analyzer software, calculating the three-dimensional parameter cortical thickness (Ct.Th), two-dimensional cross-sectional cortical area (Ct. Area) and cortical bone mineral density (BMD).

2.5. BLI measurement

Mice were imaged every week using the IVIS Lumina LT series III (PerkinElmer, Waltham, MA) to monitor tumor growth. Mice were intraperitoneally injected with luciferin (PerkinElmer 122799) at 150 mg/kg of body weight, and tumor burden in the ipsilateral side of mice was imaged 12 min after luciferin injection under 2.5 % isoflurane/air anesthesia. Bioluminescence signal was quantified in total flux in photon/second (p/s) within the region of interests (ROIs) that were selected over the hind limb with the tumor.

2.6. Behavioral pain related outcomes

Ongoing pain was defined as guarding (lifting and holding against the body) and/or reduced weight bearing on the inoculated limb with minimal contact of the paw on the floor assessed during a 5-minute observation period. For this purpose, mice were placed in raised Plexiglass chambers with a wire grid floor, acclimated to the test environment for 30 min and then their movements were videotaped. The behavioral analysis was conducted by a blinded observer. Wheel running was assessed using commercially available equipment (Med Associates, Inc., St. Albans, VT). Standard wheel running chambers contained a running wheel (18.54 cm diameter, 58.2 cm circumference) with a stainless-steel grid bar running surface located outside a 27.15 x 20.8 x 15.39 cm polycarbonate cage. Animals had free access to running wheels through a side opening in the cage. Each quarter turn of the running wheel operated a Reed switch sensor through magnets imbedded in the outer running wheelbase and were recorded via a PC-compatible interface and computer (Med Associates, Inc., St. Albans, VT). Total Reed switch closures (responses) and the time elapsed between closures (inter-response time, IRT) were recorded using the MED-PC programming language. Each running wheel chamber was isolated in a PVC sound- and light-attenuating enclosure with a ventilator fan. For experiments involving running wheel assessment, mice were housed under a reverse light: dark cycle and running wheel sessions were conducted during the dark phase of the light: dark cycle on weekdays only. Mice were allowed free access individually to running wheels for 30 min sessions on each weekday for 3 weeks. Prior to daily sessions, mice were acclimated to the behavior room for 30 min in the dark. Baseline measures for distance and optimal running rate were obtained by averaging data from the last 5 sessions of this 3-week period. In order to easily condition inter-response time (IRT) data for distance traveled in running wheels and optimal running rate analysis, a Java program was developed to truncate and transfer the data daily from the MED-PC programming language into text files that would be easily importable into SAS. Please see online content to obtain the executable files. Responses were converted to distance traveled (14.55 cm per response) and IRTs were converted to speed (14.55 cm/IRT in seconds, cm/s). For optimal velocity determination, a paradigm was developed to find the running rates that best distinguished between sham and tumor bearing animals. The optimal running rate was identified by exploring the amount of time spent running at or above certain rates using lower and upper specification limits generated by SAS Proc Capability. The optimal velocity in C57BL/6 mice was determined to be > 37.4 cm/s which was the velocity that most mice ran at least 50% of the time during the 30-minute session at baseline. Mice underwent tumor inoculation the Monday after obtaining the baseline values and running wheel activity was monitored five days a week on weekdays for 3 weeks.

2.7. Tissue preparation and immunohistochemical analysis

Mice were deeply anesthetized using isoflurane, the thorax was opened, and 0.1 M phosphate-buffered saline (PBS, pH 7.4) followed by fixative (4 % paraformaldehyde in 0.1 M PBS, pH 7.4) was perfused through the left ventricle. The femurs were removed, immersed in fixative for 24 h at 4 °C, washed for 12 h in 0.1 M PBS, decalcified in 10 % EDTA/0.1 M PBS solution for two weeks (changed to fresh solution every week), then immersed in 30 % sucrose at 4 °C for cryoprotection until ready to be sectioned. Femurs were sectioned at 25 μms on a cryostat and processed for IHC. Bone sections were labeled with an antibody against the pan-neuronal marker (PGP 9.5, 1:1000, rabbit anti-mouse, Cedarlane; cat# CL7756AP), endomucin for endothelial cells (1:100, rat anti-mouse, Santa Cruz; cat# sc-65495) CD68 for activated monocytes/macrophage (1:2000, rat anti-mouse, BioRad; cat# MCA1957GA) and GFP for labeling PCa cells (1:1000, chicken anti-mouse, Invitrogen Inc; cat# A10262). The spinal cord and dorsal root ganglia (DRG) were removed, immersed in fixative for 12 h at 4 °C and then immersed in 30 % sucrose at 4 °C for cryoprotection until ready to be sectioned. Transverse spinal cord sections were cut at 40 μms and DRG at 16 μms using a cryostat (Leica CM3050S, Leica Biosystems GmbH, Wetzlar, Germany). Spinal cord sections were stained with antibodies against the ionizing calcium binding adapter molecule 1 (IBA1, 1:1000, goat anti-rat; Abcam; cat# AB5076) for microglia and glial fibrillary acidic protein (GFAP, 1:2000, rabbit anti-bovine, Dako; cat #Z0344) for astrocytes. As markers of central sensitization, we

examined the number of cells that express phosphorylated extracellular signal regulated kinase (p-pERK, 1:1000, rabbit anti-rat, Cell Signaling; cat# 4370) and prodynorphin (pDyn, 1:500, guinea pig anti-rat Neuromics; cat# GP10110). DRG sections were labeled with antibodies against activating transcription factor 3 (ATF3, 1:500, rabbit anti-mouse, Novusbio; cat # NBP1-85816), substance P (SP, 1:500, guinea pig anti-rat, Neuromics; cat# GP14110, calcitonin gene related peptide (CGRP, 1:3000, rabbit anti-mouse, Sigma; cat# C8198) and isolectin B4 biotin conjugate (IB4, 1:1000, Sigma; cat# L2140). After incubation with primary antibodies, sections were washed three times for 10–15 min each in PBS. Subsequently, sections were incubated for 3 h at room temperature with Cy3, CY2, CY5-conjugated secondary antibody (1:500; Jackson ImmunoResearch Laboratories, Inc., West Grove, PA, USA). After washing three times, streptavidin-Cy2 was used for 1 h at room temperature and followed with another three 10-min washes. Femur, spinal cord and DRG sections were counterstained with the nuclear dye DAPI (4,6-diamidino-2-phenylindole). Finally, sections were run through 70 %, 95 %, 100 % ETOH, and xylene for 2 min each, and cover slipped with Dibutylphthalate Polystyrene Xylene (DPX).

For quantification of ATF3, SP, CGRP and IB4 in lumbar DRG, images were captured on a Nikon Eclipse Ni fluorescent microscope equipped with a Nikon DS-Qi monochrome camera and Nikon Elements Software Basic Research version 4.3. The number of positive neuronal cellular profiles was counted in a minimum of 4 randomly selected L3 and L4 sections per mouse. Counts from L3 and L4 were combined and reported as a percentage of the total neuronal profiles per L3/4 section. For quantification of pERK and dynorphin in the spinal cord, the number of cellular profiles that were positive for pERK or dynorphin were counted throughout the dorsal horn in regions corresponding to laminae I-II and III-V from a minimum of 6 lumbar spinal sections per mouse and the results were averaged similar to previous studies [8,17,41]. For GFAP and IBA1-IR, upper and lower threshold optical densities were set to match positive immunoreactivity for each marker. The optical density thresholds were applied uniformly to all sections across groups. Regions of interest were outlined corresponding to laminae I-II and laminae III-V for each section. The percent IR that fell within the optical intensity range for the corresponding region of interest (percent fractional area) was assessed in each spinal section and averaged for a minimum of 6 randomly selected sections per mouse. Individuals quantifying the images were blinded to treatment group.

2.8. Statistical analysis

The distributions of the outcome measures were checked. If outcomes were normally distributed or could be transformed to better fit the normal distribution, parametric approaches were used. If outcomes were not normally distributed and could not be transformed to approximate the normal distribution, non-parametric approaches were used. Analysis of behavior including guarding and running wheel outcomes was conducted using two-way repeated measures analysis of variance (RM ANOVA) with Student Newman Keuls (SNK) comparisons or rank based mixed effects modeling (random intercept) with group as a between subject factor, and time as a repeated-measures or within group factor. The interaction between group and time was included in the model to test whether the group effect was different by time. Analysis of disease related outcomes including BLI and radiograph scoring was conducted using Mann-Whitney rank sum test or Kruskal-Wallis one-way ANOVA on ranks due to non-normal distribution. Spinal IHC outcomes were analyzed using a two-way ANOVA with SNK comparisons with group as between subject factor and side as a within group factor. Neuronal counts in ipsilateral DRG comparing tumor bearing and sham values were analyzed using a Wilcoxon rank sum test. All hypothesis testing is two-tailed with a statistical significance threshold of $p < 0.05$. SigmaPlot version 14 or SAS version 9.4 software was used for analysis.

3. Results

3.1. Time course of tumor growth and bone remodeling in an orthotopic RM1 PCa mouse model

RM1 prostate cancer cells transduced with lentivirus co-expressing luciferase and GFP (RM1-GFP) were injected into the intramedullary space of the femur of male C57BL/6 mice (Fig. 1A). Over the course of three weeks post-inoculation, we observed a progressive increase in tumor growth evident as an increased BLI signal associated with the ipsilateral hind limb that was significantly greater on 7,14 and 20 days compared to one day post inoculation in tumor but not sham injected mice (Fig. 1B, C). During this time-period, no BLI signal above background was observed in the contralateral hind limb or other regions of the body of tumor bearing mice.

We examined radiographs from sham and RM1-GFP inoculated mice for evidence of bone remodeling and osteolysis. By day 14 and 20 after inoculation, we observed reduced opacity in radiographs of tumor bearing mice versus sham operated mice evident as loss of medullary and cortical bone predominantly in the distal aspects of the femur (Fig. 1D, E). Twenty days after tumor inoculation, mice displayed cortical bone erosion and in some cases fracture of the distal femur (Average bone score 4–5). By 21 days post tumor implantation, we observed a significant reduction in trabecular BMD in tumor bearing versus sham operated mice based on μCT analysis of the distal femur. Additional parameters were not significantly different between groups (Fig. 2B). In a subset of RM1-GFP inoculated mice, we occasionally observed extra-periosteal pathological woven bone formation along the cortical diaphysis of the ipsilateral femur which was evident in radiographs (Fig. 3A, B) and histologically (Fig. 3C). Similar to our μCT results, we observed histologically severe bone erosion and loss of trabeculae in the distal aspects of the ipsilateral femur in RM1-GFP inoculated mice (Fig. 3D) compared to the contralateral femur (Fig. 3E) and sham operated controls (data not shown).

3.2. Pain related behaviors and functional disability in tumor bearing mice

In our study, mice that received intra-femoral inoculation with RM1-GFP PCa cells exhibited spontaneous and progressively more severe guarding of the ipsilateral paw beginning day 12 through day 20 after inoculation compared to sham operated mice (Fig. 4A). Pain upon movement of the affected limb and reduced functional capacity such as reduction in ambulation are also symptoms associated with metastatic bone cancer. We examined voluntary running wheel performance of tumor bearing and sham mice for 30-minute daily running wheel sessions. Both tumor inoculated and sham operated mice exhibited transient reduction in the total distance traveled compared to baseline levels for 2 days postoperatively (Fig. 4B). Significant reductions in distance traveled were observed in RM1-GFP mice beginning 12 days post inoculation and increased through the end of the experiment (Fig. 4B). The percent of time mice ran at, or above optimal velocity was transiently reduced 1 day after inoculation in RM1-GFP mice and persistently reduced beginning 12 through 20 days post inoculation compared to baseline values (Fig. 4C)- Sham operated mice displayed only a transient reduction in percent time at optimal velocity 1 day after surgery (Fig. 4C).

3.3. Qualitative alterations in innervation, macrophage and vasculature within the tumor bearing bone of PCa mice

We conducted immunohistochemistry in the femurs from sham operated (Fig. 5A-D) and tumor bearing mice (Fig. 5E-L) to examine qualitative differences in distribution of sensory neurons, macrophage and blood vessels in relation to tumor cells within the bone. At early stages of tumor growth around the time of onset of pain related

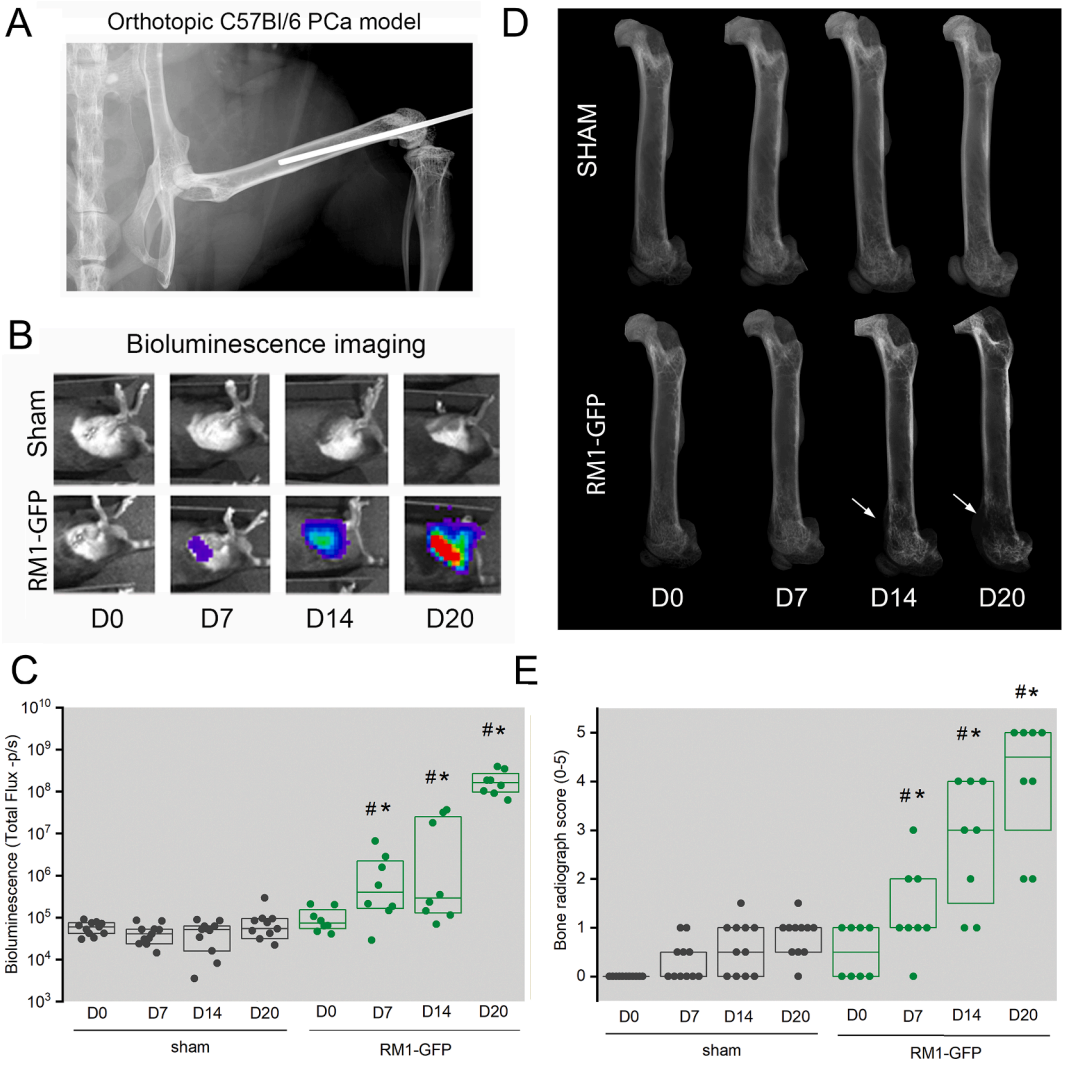

Fig. 1. Disease progression in orthotopic model of prostate cancer (PCa) induced bone pain. (A) Male C57Bl6 mice received intra-femoral injections of RM1 PCa cells transduced with luciferase and green fluorescent protein (GFP) reporter (RM1-GFP) or Hank's buffered saline for sham procedures. Needle placement was verified radiographically and following inoculation the injection site was sealed with sterile bone cement. (B) Tumor growth was monitored longitudinally with bioluminescence imaging (BLI). (C) Significant increases in BLI were observed 7,14 and 20 days post tumor cell inoculation in RM-1 injected versus sham operated mice. Data are expressed as box plots with median and 25 to 75 % quartile range # $p < 0.001$ versus sham group Mann Whitney *U* test. * $p < 0.05$, ** $p < 0.001$ versus D20 within group Friedman RM ANOVA on ranks. RM1-GFP n = 8, Sham n = 11 (D) Longitudinal radiographs of ipsilateral femur from representative sham and RM-1-GFP inoculated mice. Note osteolytic lesions present in distal aspects of femur (arrows) of tumor bearing mice. (E) Quantification of bone destruction in tumor bearing and sham mice. Data are expressed as box plots with median and 25 to 75 % quartile range # $p < 0.001$ versus sham group Mann Whitney *U* test. * $p < 0.05$, ** $p < 0.001$ versus D0 within group Friedman RM ANOVA on ranks. RM1-GFP n = 8, Sham n = 11. (For interpretation of the references to colour in this figure legend, the reader is referred to the web version of this article.)

behaviors, the tumor was confined to the intramedullary space of the femur (Fig. 5E, I). We observed PGP 9.5 positive nerve fibers in the bone marrow of sham operated and tumor inoculated mice. In sham operated mice PGP 9.5 positive axons were longitudinally oriented throughout the bone marrow (Fig. 5B). In tumor bearing mice, nerve fibers were displaced by the invading tumor cell and potentially damaged based on a fragmented appearance (Fig. 5F, J, denotated as arrows). CD68 positive macrophages were uniformly distributed throughout the bone marrow in sham operated mice (Fig. 5C). In tumor bearing mice macrophages were densely located adjacent but not within invading tumor cells (Fig. 5G, K). At the interface between the tumor and the endosteal surface of cortical bone, we commonly observed large cells that expressed CD68 which are likely osteomacs or osteoclasts [42]. Unexpectedly, many of these cells were also immunoreactive for PGP 9.5 (Fig. 5J, K, denotated as arrowheads). Similarly, endomucin positive endothelial cells lining blood vessels and sinusoids were uniformly distributed throughout the marrow of sham operated mice (Fig. 4D) but within tumor bearing mice endomucin positive vessels were displaced and congregated around the leading edge of the tumor (Fig. 5H, L). By 21 days, tumor expansion was evident throughout the intramedullary space including the distal and proximal metaphysis resulting in erosion of trabecular bone (Fig. 6A). In some instances, tumor cells could be observed eroding the cortical bone and infiltrating or colonizing between the cortical bone and periosteum (Fig. 6B, F). By 21 days, the tumor bearing bones showed extensive denervation within the bone marrow as PGP9.5 positive nerve fibers were absent in most sections (data not shown). Unlike the bone marrow, PGP 9.5 positive nerve fibers were still evident within the periosteum adjacent to infiltrating PCa cells (Fig. 6C, G), CD68 positive macrophage (Fig. 6D, E) and vasculature (Fig. 6H, I).

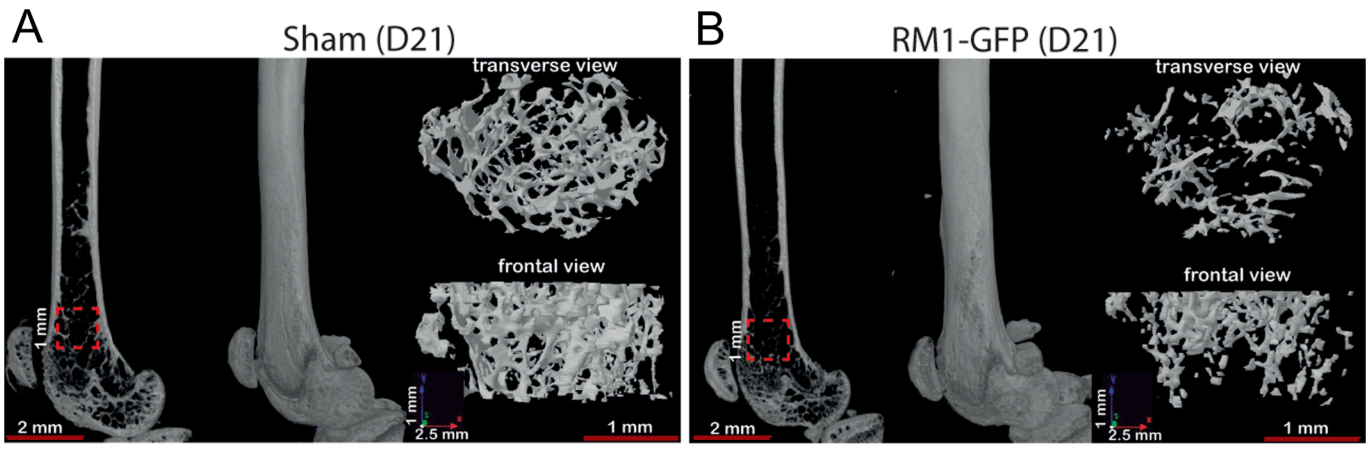

C

	Distal femur trabecular (Day 21)					Distal femur cortical (Day 21)		
	BMD (g/cm³)	BV/TV (%)	Tb. Th (mm)	Tb. N (1/mm)	Tb. Sp (mm)	BMD (g/cm³)	Ct. Th (mm)	Ct. Area (mm²)
Sham	0.17 ± 0.01	8.2 ± 0.84	0.04 ± 0.001	1.89 ± 0.16	0.19 ± 0.02	1.17± 0.01	0.19 ± 0.004	0.85 ± 0.03
RM1-GFP	0.13 ± 0.01*	6.21± 0.89	0.04 ± 0.002	1.40± 0.18	0.23 ± 0.01	1.18 ± 0.01	0.18 ± 0.004	0.81 ± 0.02

Fig. 2. μCT scans of femurs from sham and tumor bearing mice including 2D slice and 3D image of entire femur and distal metaphysis (insets, A). Quantification of key μCT outcomes (B) indicate loss of trabeculae in the distal femur due to osteolysis. Student's *t*-test *p < 0.05 versus Sham values. Sham n = 8, RM1-GFP n = 8.

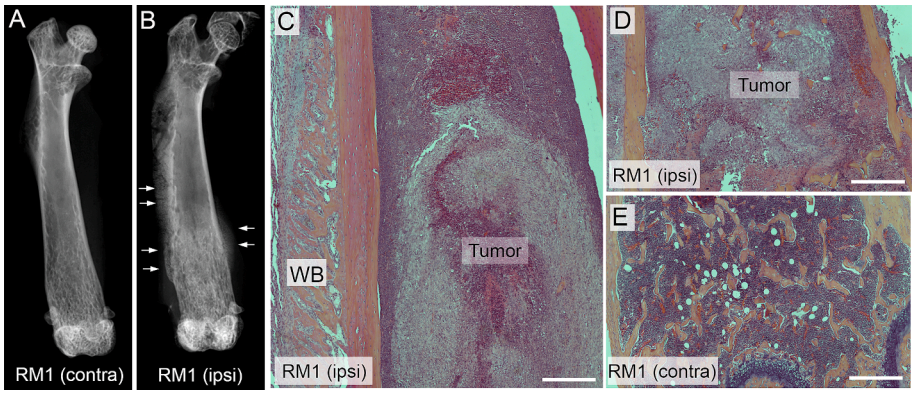

Fig. 3. Tumor bearing mice develop extra-periosteal osteosclerotic and metaphyseal osteolytic lesions. Radiographs of the contralateral (A) and ipsilateral (B) femur of a mouse 21 days after implantation with RM1-GFP PCa cells. Arrows indicate sites of extra-periosteal bone formation. Hematoxylin and eosin stain of the tumor bearing femur of an RM1-GFP implanted mouse at the mid-diaphysis (C) and distal metaphysis (D). Note woven bone (WB) formation of the cortical bone and near complete erosion of trabeculae in the distal metaphysis compared to the contralateral femur (E). Scale bar in C = 500 μm and D and E = 475 μm.

3.4. Increased ATF3 expression and upregulation of the neuropeptides SP and CGRP in the ipsilateral DRG of tumor bearing mice

We examined the ipsilateral L3/4 DRG of tumor bearing and sham operated mice at 21 days following surgery for evidence of neurochemical changes in the DRG associated with later stages of disease progression. The percentage of ATF3 + sensory neurons in the ipsilateral DRG was significantly greater in tumor bearing versus sham operated mice (Fig. 7A-C; 9.4 +/- 0.6 % RM1-GFP vs. 3.3 +/- 0.23 % Sham). The percentage of SP (Fig. 7D-F; 20.3 +/- 1.0 % RM1-GFP vs. 13.0 +/- 0.56 % Sham) and CGRP (Fig. 7G-I; 43.8 +/- 1.2 % RM1-GFP vs. 39.1 +/- 0.9 % Sham) positive neurons were also increased in tumor bearing versus sham operated mice. The percentage of IB4 positive neurons was not different between groups (Fig. 7J-L) (27.9 +/- 1.0 % RM1-GFP vs. 26.7 +/- 1.7 % Sham).

3.5. Spinal central sensitization and glial activation are present in mice with RM1-GFP PCa induced bone pain

RM1-GFP inoculated mice displayed upregulation of dynorphin in interneurons within deep laminae (III-V) of the ipsilateral spinal cord compared to sham operated mice (Fig. 8A-C). We also observed a significant increase in cellular profiles immunoreactive for pERK in superficial (I-II) but not deep (III-V) laminae (Fig. 8D-F).

We observed a significant increase in astrocyte activation in the spinal cord of tumor bearing mice compared to sham operated mice (Fig. 9A-C). Within the superficial spinal cord there was a bilateral increase in GFAP-IR, however in deeper laminae the significant increase in GFAP-IR was confined to the side of the spinal cord ipsilateral to tumor injection. Microglial activation or IBA1-IR was not significantly different between tumor bearing and sham operated mice 21 days post implantation (Fig. 9D-F).

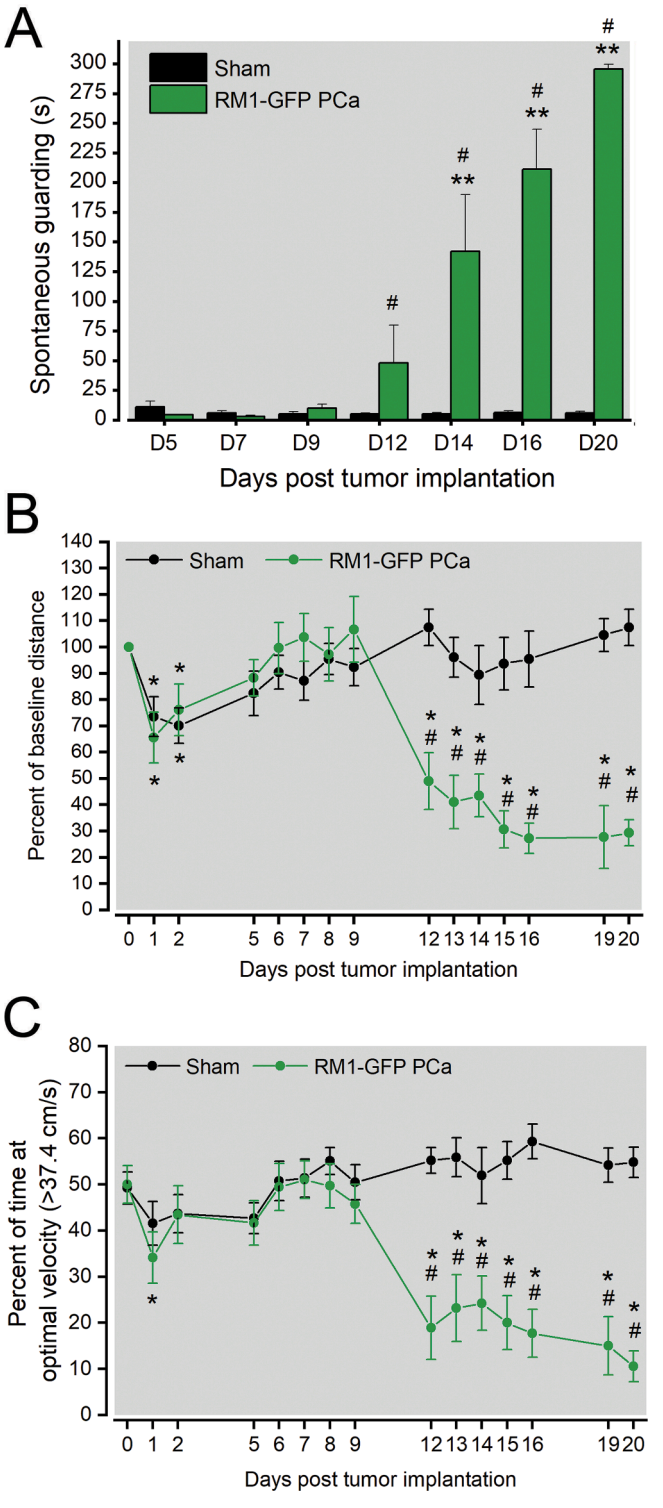

(caption on next column)

Fig. 4. Time course of pain related behaviors in tumor bearing mice. In mice following intra-femoral injection of RM1-GFP PCa cells ongoing pain is evident as progressive increase in duration of guarding of the tumor bearing hindlimb during a 5-minute observation period compared to mice with sham procedure (A). Data are mean ± SEM. Two-way RM ANOVA with SNK comparisons. Group effect: $p < 0.001$, Time effect: $p < 0.001$ and Group x Time: $p < 0.001$, #P < 0.001 versus sham values and ** $p < 0.001$ vs D7. Sham n = 11, RM1-GFP n = 8. Tumor bearing mice also displayed progressive impairment in running wheel performance. The distance mice ran during daily 30-minute sessions was reduced beginning 12 days post inoculation compared to sham mice (B). Data are mean ± SEM. Mixed effects modeling (rank based) Group effect: $p < 0.001$, Time effect: $p < 0.001$ and Group x Time: $p < 0.001$, #P < 0.001 versus sham values and ** $p < 0.001$ vs D7. Sham n = 12, RM1-GFP n = 12. Similarly, the percentage of time at an optimal velocity was reduced progressively compared to sham mice beginning 12 days post inoculation. Mixed effects model (rank based). Data are mean ± SEM. Group effect: $p < 0.001$, Time effect: $p < 0.001$ and Group x Time: $p < 0.001$, #P < 0.001 versus sham values and ** $p < 0.001$ vs D7. Sham n = 12, RM1-GFP n = 12.

4. Discussion

Bone pain is a significant and debilitating symptom associated with metastatic prostate cancer. Despite significant progress in the past 20 years developing animal models of CIBP, our understanding of mechanisms that govern this pain state are incomplete. The pain research field still lacks a well characterized immunocompetent mouse model of prostate cancer induced bone pain which is essential for evaluating the ability of immune modulating therapies to reduce pain and disease progression in metastatic PCa. In the current study, we demonstrate that implantation of C57BL/6 mice with RM1-GFP cells in the femur results in osteolytic and osteoblastic bone remodeling, progressive pain related behaviors indicative of ongoing and movement-evoked pain, increased markers of central sensitization in the spinal cord and cellular reorganization in the bone microenvironment.

4.1. Characterization of pain related behaviors following orthotopic implantation of RM1-GFP PCa cells

To date, only a few studies have used the RM1 cell line to examine mechanisms of bone cancer pain. Previous studies observed progressive increases in mechanical and thermal hyperalgesia within the paw of the tumor bearing limb following intra tibial [33] or intra femoral injection of RM1 cells [34]. Notably, these prior studies focused primarily on hypersensitivity referred to the tumor bearing paw rather than spontaneous or movement evoked pain. This is important as preclinical studies have established that the mechanisms that govern ongoing or spontaneous pain related behaviors in bone cancer models may be distinct from those that drive referred hypersensitivity in the skin [43,44]. Notably, in the current study we observed robust and progressive increase in the time spent guarding or elevating the tumor bearing limb which is reminiscent of ongoing cancer pain observed clinically. Another notable characteristic of metastatic bone pain is the exacerbation of pain associated with movement that often results in avoidance of daily activities and functional disability [45,46]. Rodent studies have explored several outcomes to assess movement or functional impairment in bone cancer pain models including impairment in burrowing behavior and disruption of gait [26,35,47]. The most widely used outcome for assessing movement evoked pain is limb use score which consists of evaluating the extent to which the mouse utilizes the tumor bearing limb during voluntary movement by blinded observers with "4″ equaling normal ambulation and "0" equaling paralysis/no use of the limb [38,43,48]. While this is a widely used and reproducible method across laboratories a significant limitation is the subjective nature of this outcome. More objective and quantitative methods are needed. We evaluated voluntary running wheel longitudinally in tumor bearing and sham operated mice as part of the current study. We observed a biphasic reduction in the

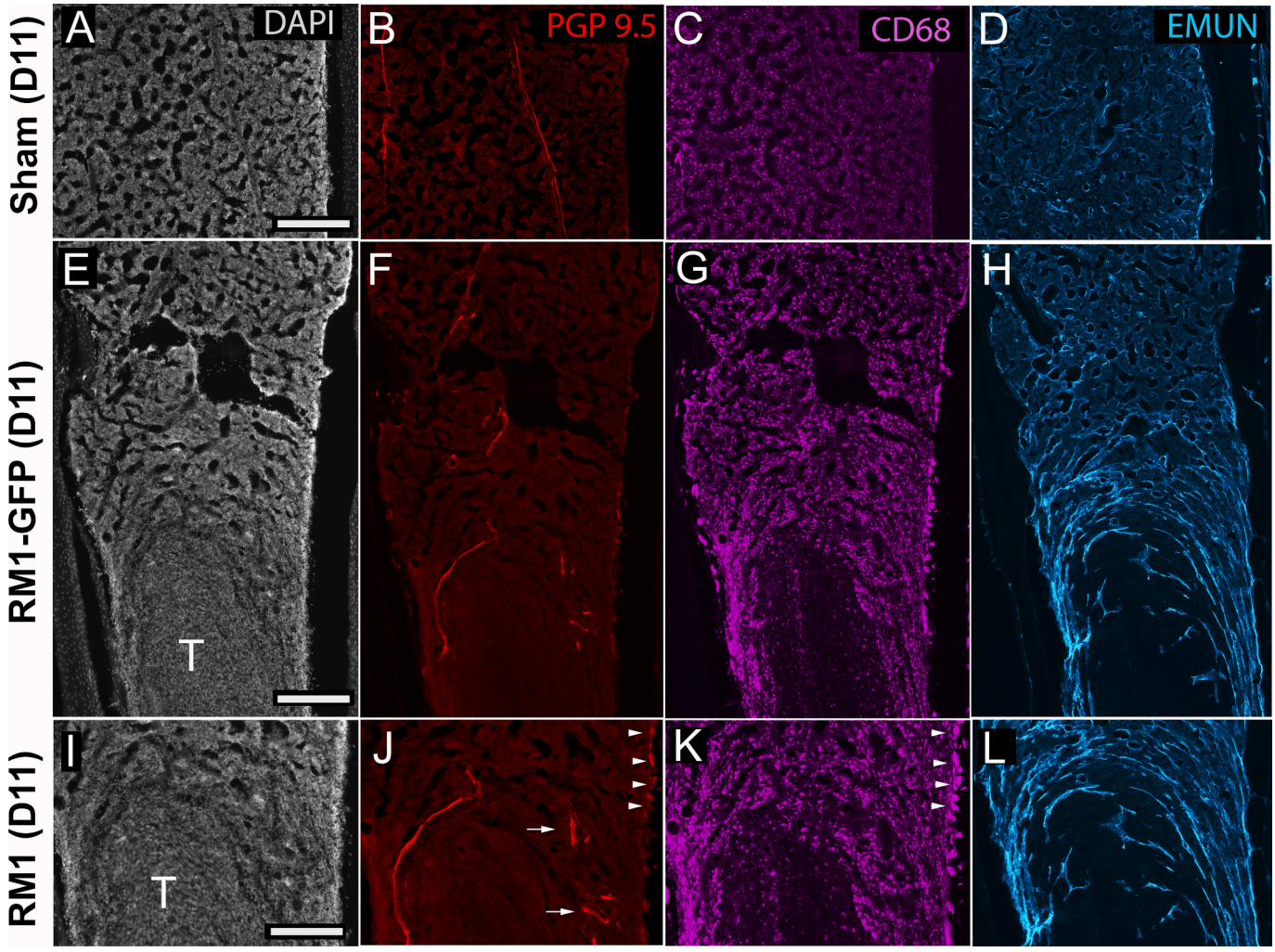

Fig. 5. Cellular alterations in the bone microenvironment at early stages of tumor growth. Sections of sham-operated (A – D) and tumor-bearing mouse femur (E-L) obtained D11 post inoculation were counterstained with DAPI (white, A, E, I) and labeled immunohistochemically with the pan-neuronal marker PGP 9.5 (red, B, F, J); CD68 (purple, C, G, K) for activated macrophage/osteoclasts and endomucin (EMUN, blue, D, H, L) to visualize endothelial cells in blood vessels and sinusoids. DAPI staining revealed the presence of tumor cells within the intramedullary space of PCa injected mice ("T" in E, I). In sham operated mice, PGP 9.5 IR nerve fibers were oriented longitudinally throughout the bone marrow (A). In tumor bearing mice, nerve fibers were displaced adjacent to the tumor or displayed a more fragmented appearance (F, J, arrows). In tumor bearing femurs, PGP 9.5 immunoreactivity was also present in cells with the appearance of activated osteoclasts lining the endosteal surface that colocalized with CD68 (arrowheads, J. K). Unlike sham operated mice which displayed unform distribution of CD68-IR macrophage and EMUN-IR vessels throughout the bone marrow (C, D) in tumor bearing mice activated macrophage (G, K) and vessels (H, L) possessed a disoriented and denser appearance at the leading edge or adjacent to the tumor. Scale bar A, E = 450 μm; I = 200 μm. (For interpretation of the references to colour in this figure legend, the reader is referred to the web version of this article.)

percentage of baseline distance traveled as well as the time spent at a predetermined optimal velocity. Both tumor bearing and sham operated mice displayed a transient reduction in running wheel performance immediately after intra-femoral injection which recovered to baseline values within 7 days. This initial impairment was likely due to tissue injury and inflammation resulting from surgery. By day 12 post tumor inoculation, tumor bearing mice displayed clear progressive impairment in running wheel performance. Notably, this time point coincided with the emergence of guarding behavior in the same mice and prior to evidence of skeletal fracture or pervasive tumor burden which typically did not occur until between 14 and 20 days post inoculation. We propose that reductions in running wheel performance reflect in part avoidance due to movement related pain as has been observed in other preclinical pain studies [49]. However, since voluntary running wheel activity is a motivated behavior in rodents, reductions in running wheel performance might also be indicative of an anxio-depressive state with tumor bearing mice less inclined to participate in the activity [50]. In future studies, we will determine if the impairment in wheel performance is reversible or preventable with common analgesics or by inhibiting sensory neurons that innervate the bone.

4.2. Characterization of bone remodeling and disease progression following orthotopic implantation of RM1-GFP cells

It is also essential to carefully examine tumor growth and bone remodeling longitudinally in animal models of CIBP in order to properly interpret therapeutic efficacy as several analgesics have been shown to impact tumor growth and tumor induced bone remodeling in beneficial [9,29,51] and adverse ways [52]. In the current study, we observed detectable differences in BLI levels and radiological evidence of osteolytic bone lesions as early as 7 days post tumor inoculation - a few days prior to the development of spontaneous guarding behavior and impairment of running wheel performance. We also observed a predominantly osteolytic phenotype with loss of trabeculae in the distal aspects of the femur and at later stages extra-periosteal aberrant woven bone formation. This is consistent with previous studies that have

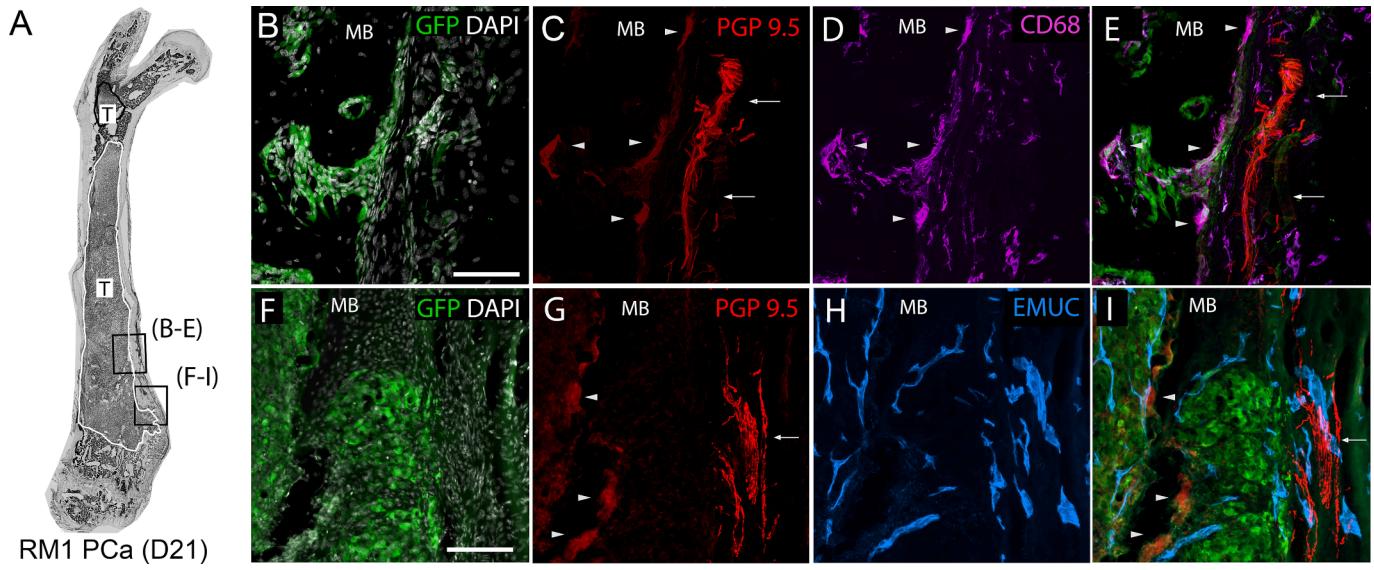

Fig. 6. Periosteal nerve sprouting occurs adjacent to RM1-GFP prostate cancer cells within the periosteum of tumor bearing mice at later stages of tumor growth. Tumor-bearing mouse femur were decalcified and sectioned for immunohistochemistry (IHC). Left panel depicts a RM1-GFP femur at 21 days post inoculation. Sections were counterstained with DAPI revealing dense cellularity associated with the presence of tumor (T) throughout nearly 90 % of the intramedullary space of the femur (A). High power confocal images of regions of the tumor bearing femur labeled with DAPI (white) and green fluorescent protein (GFP, green, B, F); an antibody against the pan-neuronal marker PGP 9.5 (red, C, G); CD68 (purple, D) a cell surface antigen present predominantly on activated macrophage/osteoclasts or endomucin (EMUC, blue, H) a marker of vascular endothelial cells and merged image (E, I) Arrowheads indicate PGP positive macrophage/osteoclasts and arrows indicate PGP positive nerve fiber bundles. Scale bar A, B = 50μms. MB = mineralized bone. (For interpretation of the references to colour in this figure legend, the reader is referred to the web version of this article.)

utilized parental or a bone trophic variant of the RM1 cell line [53,54]. Notably, we did not observe woven bone formation within the intramedullary space as observed in a well described ACE-1 CIBP model [28]. One reason for this may be the use of immunocompromised athymic mice in the ACE-1 model or phenotypical differences between the PCa cell lines. Notably, extra periosteal rather than intramedullary bone formation is clinically more common in patients with metastatic prostate cancer [55]. The time course of these changes suggests that RM1 cell line is characterized by an initial osteolytic phase with erosion of predominantly the trabecular bone within the distal metaphysis. This is followed by the development of extra-periosteal bone formation at a later stage likely in response to tumor invasion into the periosteum and adjacent soft tissue.

4.3. Cellular reorganization in the bone microenvironment, DRG and spinal cord in CIBP

We made several observations of anatomical changes in the periphery, DRG and spinal cord that accompanied PCa induced pain behaviors. We observed an initial displacement of nerve fibers and vasculature within the intramedullary space at the onset of pain behaviors (D11). We also observed potential damage to terminals of sensory neurons in the bone marrow as some fibers displayed a fragmented appearance suggesting that as the tumor burden increases within the bone marrow there is damage and injury to the distal terminals of sensory and sympathetic neurons [17]. We observed dense infiltration of CD68 IR cells around the tumor margin but not within the tumor. These cells may comprise a population of activated macrophages and are potential contributors to CIBP as a source of proinflammatory cytokines including TNF-α, IL-6, and prostaglandins with established roles in sensitizing sensory neurons that innervate bone [2,56,57]. Large CD68 positive cellular profiles, indicative of activated osteoclasts, were present along the endosteal surface of the tumor bearing bone. We also observed PGP-IR in some of these bone lining cells. PGP 9.5 protein is a ubiquitin carboxyl-terminal hydrolase (UCHL1) that is widely used as a neuron specific marker [58]. However, recent studies demonstrate that UCHL1 can be expressed in osteoclasts and may negatively regulate osteoclastogenesis [59], although a potential role in PCa induced bone remodeling is unknown. At later time points, we observed dense bundles of PGP9.5 positive nerve fibers within the periosteum adjacent to invading tumor cells suggestive of pathological sprouting observed in other bone cancer models [19–21] and observed clinically in cancer patients with bone metastasis [23,60]. We did not examine in detail the distribution and phenotype of these neurons; however, prior studies have shown that the periosteum is comprised of a mesh work of predominantly myelinated and unmyelinated peptidergic (calcitonin-gene related peptide, CGRP) nociceptive afferents [6] that are positioned to be significant contributors to cancer induced bone pain resulting from distortion of the periosteum as the tumor compresses the periosteal lining or from mechanical stimulation [61].

Prior studies have documented unique neurochemical plasticity in the DRG and spinal cord in mouse models of bone cancer pain [2]. ATF3 is a stress induced transcription factor that is upregulated in response to nerve injury [62], but less frequently under inflammatory conditions [63]. In agreement with prior studies in sarcoma and myeloma induced bone pain models [17,23,52], we observed an upregulation of ATF3 in nearly 10 % of sensory neurons in the DRG ipsilateral to the tumor bearing femur suggesting tumor induced neuronal injury occurs as the tumor occupies the bone marrow and invades into the adjacent periosteum. Conversely, the excitatory neuropeptides SP and CGRP are often decreased in the DRG after nerve injury [3,64] while peripheral inflammation increases SP and CGRP levels [65,66]. In the current study, we observed a significant increase in the percentage of SP and CGRP positive neurons in the ipsilateral DRG of tumor bearing mice. In prior studies, no change in the levels of SP and CGRP were reported in a mouse model of bone cancer due to sarcoma [17]. More recent studies in models of breast and lung cancer induced bone pain report increased levels of these neuropeptides in ganglia [67,68]. Thus, the expression of these neuropeptides may be tumor type dependent. Collectively, this evidence supports that bone cancer pain is a mixture of neuropathic and

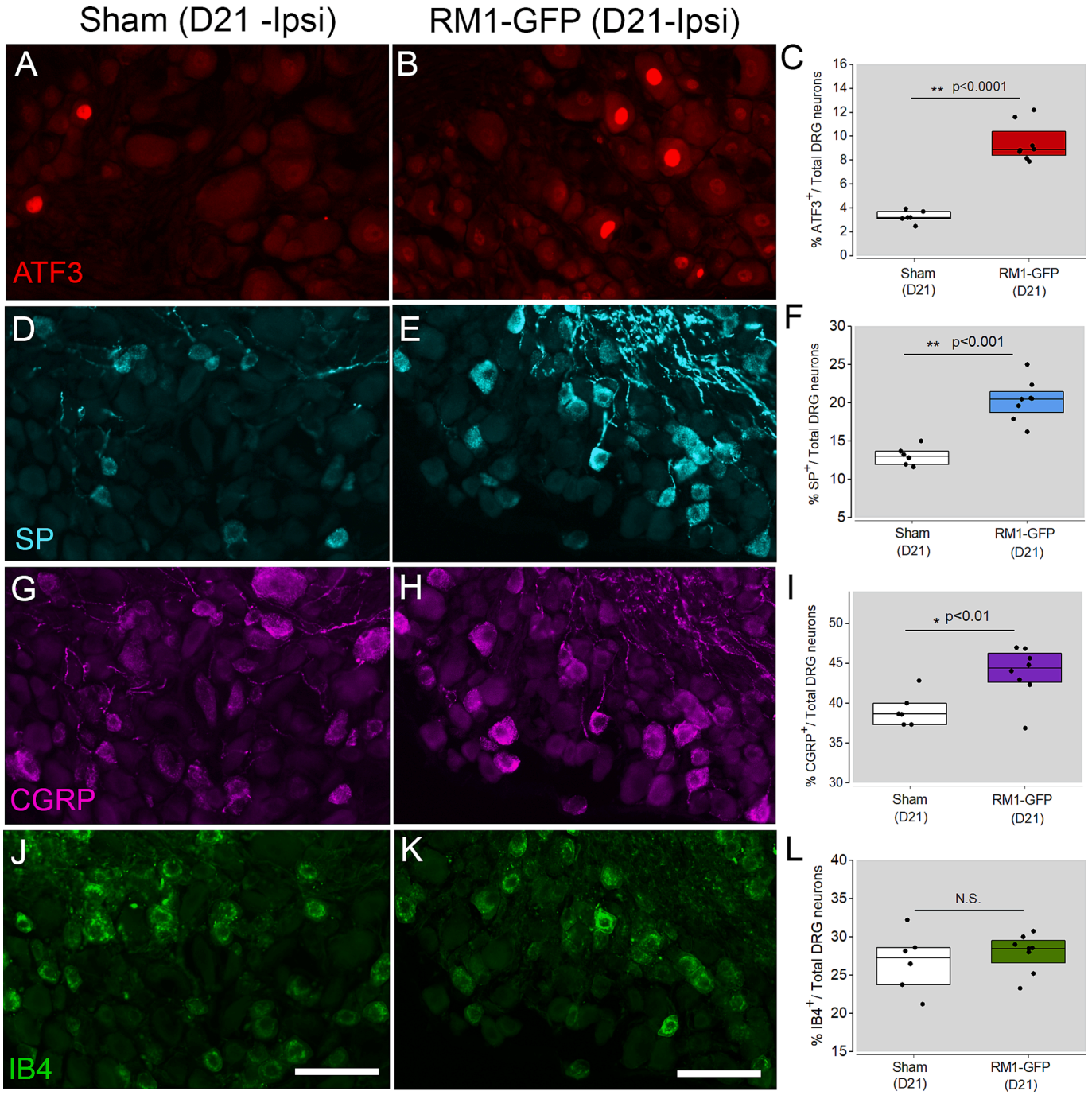

Fig. 7. Alterations in the neurochemical phenotype indicative of neuronal injury and inflammation occur in the ipsilateral DRG of tumor bearing mice 21 days post inoculation. Representative images in the ipsilateral L3 DRG from sham operated (A, D, G, J) and RM1-GFP tumor bearing mice (B, E, H, K) for the neuronal injury marker activating transcription factor 3 (ATF3, red A,B); substance P (SP, blue, D,E); calcitonin gene related peptide (CGRP, purple, G,H) and isolectin B4 (IB4, green). The percentage of ATF3-IR (C), SP-IR (F) and CGRP-IR (I) but not IB4-IR (L) neurons were increased in the ipsilateral L3/4 DRG of RM1-GFP tumor bearing compared to sham operated mice. Data presented as median with 25th and 75th quartiles. Sham n = 6, RM1-GFP n = 8. Scale bar in J, K = 100 μms. (For interpretation of the references to colour in this figure legend, the reader is referred to the web version of this article.)

inflammatory pain conditions with regions of tumor induced nerve injury and areas of enhanced immune activation and inflammation within the bone tumor microenvironment.

The neuroplastic changes observed in the periphery and DRG would be predicted to result in increased release of pronociceptive neurotransmitters from spinal terminals of primary afferents and alterations in synaptic function within the dorsal spinal cord contributing to central sensitization of second order neurons [69,70]. In the current study, we observed upregulation of dynorphin levels within a subpopulation of interneurons as observed in previous mouse models of bone cancer pain [4,8,10,17] and nerve injury [71,72]. Similarly, upregulation of phosphorylated ERK has been reported to contribute to pain related behaviors in several persistent pain states including bone cancer [73,74]. We observed a pronounced astrocyte activation in superficial (I-II) and deeper laminae (III-V) of the spinal cord but not microglia. There is some evidence that pharmacological approaches that target astrocyte signaling can reduce bone cancer pain related behaviors in particular mechanical hypersensitivity in the ipsilateral hindpaw [34] while the

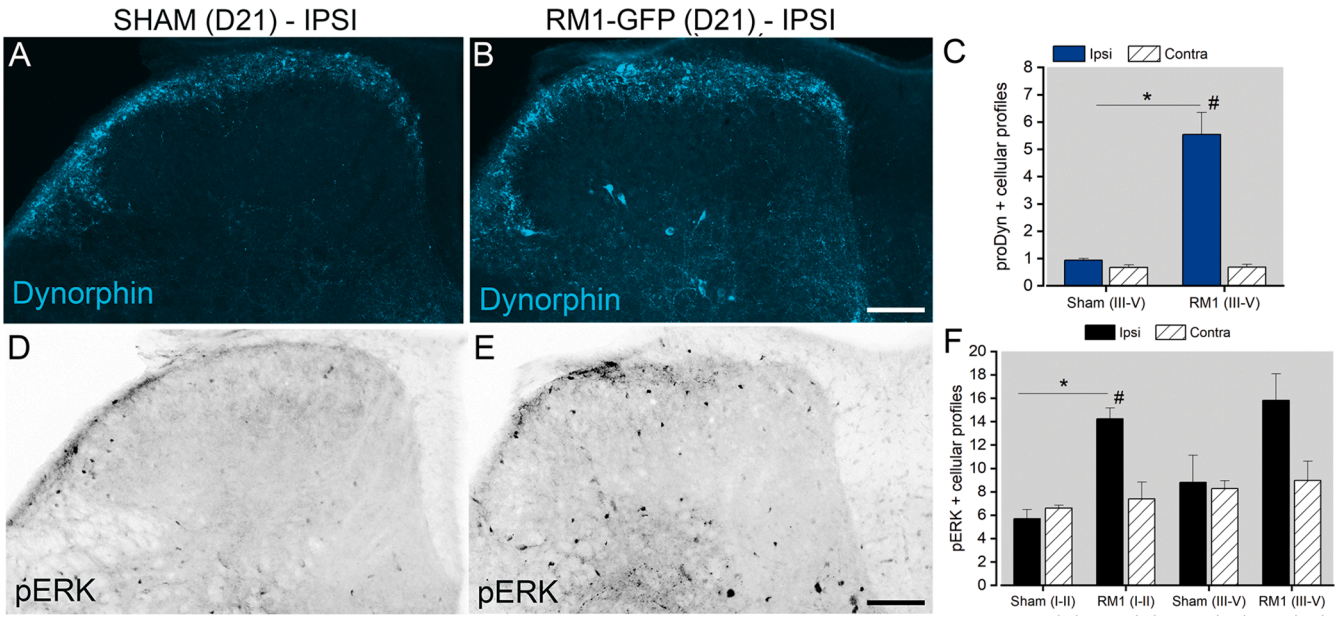

Fig. 8. Neurochemical changes associated with central sensitization are present in the ipsilateral spinal cord of tumor bearing mice 21 days post injection. Representative images of proDynorphin-IR (A) and pERK-IR (D) in the ipsilateral spinal cord of sham and RM1-GFP PCa injected mice. Dynorphin-IR cellular profiles are increased in the ipsilateral deep dorsal horn of tumor bearing mice (B), pERK-IR profiles are increased in superficial but not deep dorsal horn of tumor bearing mice (D). Data are expressed as mean ± SEM. Two-way RM ANOVA with SNK comparisons. For Dyn (II-V): Group effect: $p = 0.003$, Side effect: $p = 0.002$ and Group x Side: $p = 0.004$ # $p < 0.001$ vs contra, * $p < 0.001$ vs sham. For pERK (I-II): Group effect: $p = 0.003$, Side effect: $p = 0.042$ and Group x Side: $p = 0.011$ # $p < 0.001$ vs contra, * $p < 0.001$ vs sham. For pERK (III-IV): Group effect: $p = 0.107$, Side effect: $p = 0.122$ and Group x Side: $p = 0.182$. Sham n = 3, RM1-GFP n = 8. Fluorescent images of pERK-IR in panels D &E were converted to gray scale and inverted to better reveal labeling.

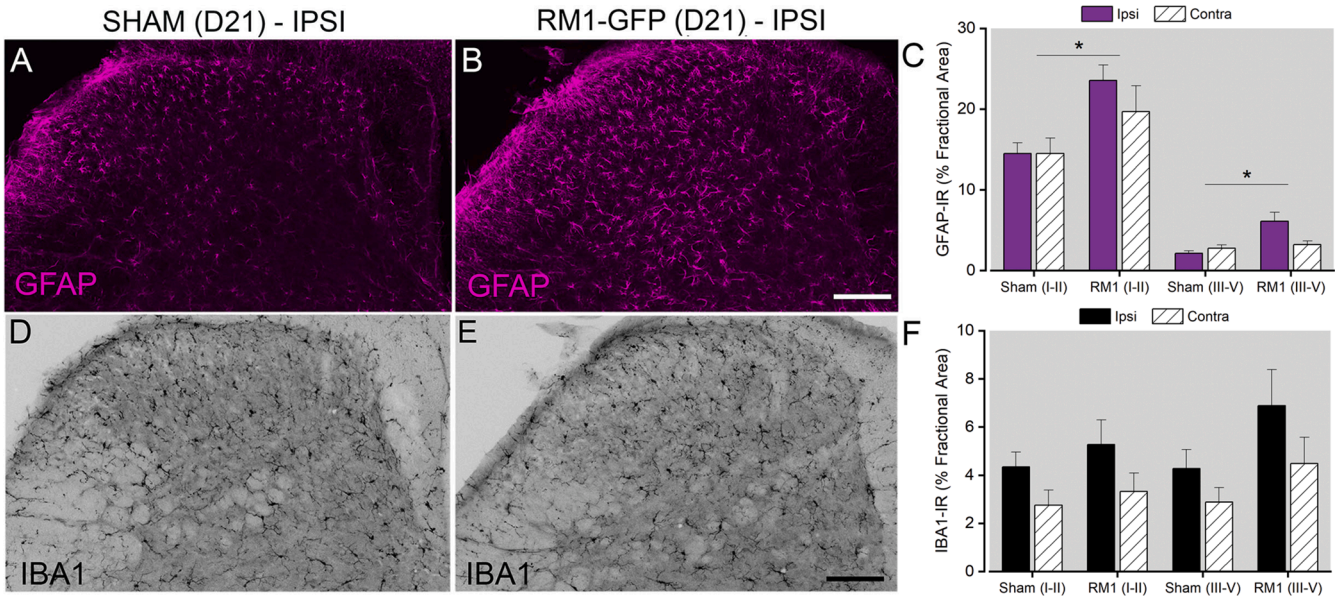

Fig. 9. Alterations in spinal glial plasticity were assessed with antibodies against GFAP for astrocytes (A) and IBA1 for microglial (C) in the ipsilateral spinal cord of tumor bearing mice 21 days post inoculation. GFAP-IR is increased in the ipsilateral deep dorsal horn of tumor bearing mice (B). IBA1-IR was not significantly greater in tumor bearing vs sham mice, however there was a general increase in IBA1-IR in the ipsilateral side. Two-way ANOVA with SNK comparisons. For GFAP (I-II): Group effect: $p = 0.031$, Side effect: $p = 0.53$ and Group x Side: $p = 0.53$. For GFAP (III-V): Group effect: $p = 0.016$, Side effect: $p = 0.127$ and Group x Side: $p = 0.034$ # $p < 0.05$ vs contra, * $p < 0.003$ vs sham. For iBA1 (I-II): Group effect: $p = 0.485$, Side effect: $p = 0.112$ and Group x Side: $p = 0.868$. For IBA1 (III-IV): Group effect: $p = 0.184$, Side effect: $p = 0.230$ and Group x Side: $p = 0.744$. Sham n = 3, RM1-GFP n = 7. Fluorescent images of IBA1-IR in panels D &E were converted to gray scale and inverted to better reveal labeling.

contribution of microglia is more varied across studies. Whether or not microglia contribute to CIBP may be dependent on sex, strain and type of cancer [75,76]. Importantly, examination of these spinal changes is a valuable outcome for screening the potential of novel analgesics to treat CIBP as several therapies that reduced pain related behaviors in mouse models of bone cancer effectively reduced these indices of central sensitization in preclinical studies [8,10,17,77,78].

4.4. Relevance and application of immunocompetent mouse models of bone cancer pain for the study of tumor microenvironment and sensory neuron tumor interactions

Animal models that reliably reproduce human disease are valuable for examining mechanisms and treatment strategies for bone metastatic bone cancer. Several models have been developed that involve engraftment of human cell lines into immunocompromised rodents [25,79]. The use of human cell lines more closely reflects the histopathology and genetic makeup found in human neoplasms and implantation in immune deficient mice is valuable for determining the genetic and cellular alterations that are necessary for promoting survival and growth of human cancer cells within the bone microenvironment. A notable limitation is that these studies require the use of nude athymic or severe combined immunodeficient (SCID) rodents that have a compromised adaptive immune system lacking T and B cells. Additionally, the innate immune system including natural killer cells and macrophages may also be altered in these mice [80]. Because innate immune cells including tumor associated macrophages are integrally involved in contributing to tumor cell proliferation, aberrant bone remodeling [54] and potentially bone pain [29] immunocompromised rodents may not be adequate for mechanistic understanding of the cellular interactions that drive bone cancer pain and metastatic disease [79]. Several syngeneic mouse models have already been developed to fill this gap including orthotopic models of sarcoma (2472) [4], breast (66.1, 4 T1) [51,81], lung (LL2) [82], and more recently prostate (RM1 and B6 Hi-Myc) [33–35] cancer in select strains of mice. Importantly, the current model is on a C57BL/6 background strain which is commonly used strain for genetically modified mice and pain studies. There is also emerging research using transgenic mice to label and modulate molecularly defined populations of sensory neurons within bone and joints [83]. An important future line of research in this model will be to better define the regional distribution and plasticity of subpopulations of molecularly defined sensory neurons in the bone tumor microenvironment and assess their contribution to bone cancer pain.

5. Conclusion

This immunocompetent mouse PCa bone pain model will be useful when combined with cell type specific recombinase (Cre/Flpo) driver mice to examine tumor, immune cell and sensory neuron interactions in the bone microenvironment and their role in pain and disease progression associated with bone cancer.

6. Funding and disclosures

Supported in part by DOD W81XWH-17–1-0542 (Peters), DOD W81XWH-17–1-0541 (Shiozawa), DOD W81XWH-19–1-0045 (Shiozawa), NCI R01CA238888 (Shiozawa), NCI R44CA203184 (Shiozawa), METAvivor Research Award (Shiozawa), and NCI P30CA012197. Yusuke Shiozawa has received research funding from TEVA Pharmaceuticals, but not relevant to this study. The remaining authors declare no conflicts of interest.

CRediT authorship contribution statement

Juan Miguel Jimenez-Andrade: Conceptualization, Methodology, Formal analysis. **Martha B. Ramírez-Rosas:** Investigation, Methodology, Formal analysis. **Sun Hee Park:** Investigation, Methodology, Formal analysis. **Renee Parker:** Investigation, Methodology, Formal analysis. **Matthew R. Eber:** Investigation, Methodology, Formal analysis. **Rebecca Cain:** Investigation, Methodology, Formal analysis. **Mary Newland:** Investigation, Methodology, Formal analysis. **Fang-Chi Hsu:** Investigation, Methodology, Formal analysis. **Carol A. Kittel:** Investigation, Methodology, Formal analysis. **Thomas J. Martin:** Methodology, Formal analysis. **Enriqueta Muñoz-Islas:** Investigation, Methodology, Formal analysis. **Yusuke Shiozawa:** Conceptualization, Methodology, Formal analysis, Funding acquisition. **Christopher M. Peters:** Conceptualization, Methodology, Formal analysis, Funding acquisition.

Declaration of Competing Interest

The authors declare that they have no known competing financial interests or personal relationships that could have appeared to influence the work reported in this paper.

Acknowledgements

This work was supported by the National Cancer Institute's Cancer Center Support Grant award number P30-CA012197 issued to the Wake Forest Baptist Comprehensive Cancer Center. The authors wish to acknowledge the support of the Wake Forest Baptist Comprehensive Cancer Center Cell Engineering Shared Resource and Flow Cytometry Shared Resource, supported by the National Cancer Institute's Cancer Center Support Grant award number P30-CA012197. The content is solely the responsibility of the authors and does not necessarily represent the official views of the National Cancer Institute and the Department of Defense.

References

[1] P.W. Mantyh, Bone cancer pain: from mechanism to therapy, Curr. Opin. Support Palliat Care 8 (2) (2014) 83–90.
[2] A.N. Lozano-Ondoua, A.M. Symons-Liguori, T.W. Vanderah, Cancer-induced bone pain: mechanisms and models, Neurosci. Lett. 557 Pt A (2013) 52-9.
[3] P. Honore, S.D. Rogers, M.J. Schwei, J.L. Salak-Johnson, N.M. Luger, M.C. Sabino, D.R. Clohisy, P.W. Mantyh, Murine models of inflammatory, neuropathic and cancer pain each generates a unique set of neurochemical changes in the spinal cord and sensory neurons, Neuroscience 98 (3) (2000) 585–598.
[4] M.J. Schwei, P. Honore, S.D. Rogers, J.L. Salak-Johnson, M.P. Finke, M. L. Ramnaraine, D.R. Clohisy, P.W. Mantyh, Neurochemical and cellular reorganization of the spinal cord in a murine model of bone cancer pain, J. Neurosci. 19 (24) (1999) 10886–10897.
[5] D.B. Mach, S.D. Rogers, M.C. Sabino, N.M. Luger, M.J. Schwei, J.D. Pomonis, C. P. Keyser, D.R. Clohisy, D.J. Adams, P. O'Leary, P.W. Mantyh, Origins of skeletal pain: sensory and sympathetic innervation of the mouse femur, Neuroscience 113 (1) (2002) 155–166.
[6] C.D. Martin, J.M. Jimenez-Andrade, J.R. Ghilardi, P.W. Mantyh, Organization of a unique net-like meshwork of CGRP+ sensory fibers in the mouse periosteum: implications for the generation and maintenance of bone fracture pain, Neurosci. Lett. 427 (3) (2007) 148–152.
[7] P. Mantyh, Bone cancer pain: causes, consequences, and therapeutic opportunities, Pain 154 (Suppl 1) (2013) S54–S62.
[8] C.M. Peters, T.H. Lindsay, J.D. Pomonis, N.M. Luger, J.R. Ghilardi, M.A. Sevcik, P. W. Mantyh, Endothelin and the tumorigenic component of bone cancer pain, Neuroscience 126 (4) (2004) 1043–1052.
[9] B. Remeniuk, T. King, D. Sukhtankar, A. Nippert, N. Li, F. Li, K. Cheng, K.C. Rice, F. Porreca, Disease modifying actions of interleukin-6 blockade in a rat model of bone cancer pain, Pain 159 (4) (2018) 684–698.
[10] M.A. Sevcik, J.R. Ghilardi, C.M. Peters, T.H. Lindsay, K.G. Halvorson, B.M. Jonas, K. Kubota, M.A. Kuskowski, L. Boustany, D.L. Shelton, P.W. Mantyh, Anti-NGF therapy profoundly reduces bone cancer pain and the accompanying increase in markers of peripheral and central sensitization, Pain 115 (1–2) (2005) 128–141.
[11] L.M. Slosky, N.M. BassiriRad, A.M. Symons, M. Thompson, T. Doyle, B.L. Forte, W. D. Staatz, L. Bui, W.L. Neumann, P.W. Mantyh, D. Salvemini, T.M. Largent-Milnes, T.W. Vanderah, The cystine/glutamate antiporter system xc- drives breast tumor cell glutamate release and cancer-induced bone pain, Pain 157 (11) (2016) 2605–2616.
[12] J.R. Ghilardi, H. Rohrich, T.H. Lindsay, M.A. Sevcik, M.J. Schwei, K. Kubota, K. G. Halvorson, J. Poblete, S.R. Chaplan, A.E. Dubin, N.I. Carruthers, D. Swanson, M. Kuskowski, C.M. Flores, D. Julius, P.W. Mantyh, Selective blockade of the capsaicin receptor TRPV1 attenuates bone cancer pain, J. Neurosci. 25 (12) (2005) 3126–3131.
[13] T. Yoneda, M. Hiasa, Y. Nagata, T. Okui, F. White, Contribution of acidic extracellular microenvironment of cancer-colonized bone to bone pain, Biochim. Biophys. Acta 1848(10 Pt b) (2015) 2677–2684.
[14] M. Hiasa, T. Okui, Y.M. Allette, M.S. Ripsch, G.H. Sun-Wada, H. Wakabayashi, G. D. Roodman, F.A. White, T. Yoneda, Bone pain induced by multiple myeloma is reduced by targeting V-ATPase and ASIC3, Cancer Res. 77 (6) (2017) 1283–1295.
[15] T. Yoneda, M. Hiasa, Y. Nagata, T. Okui, F.A. White, Acidic microenvironment and bone pain in cancer-colonized bone, Bonekey Rep. 4 (2015) 690.
[16] M. Diaz-delCastillo, D. Kamstrup, R.B. Olsen, R.B. Hansen, T. Pembridge, B. Simanskaite, J.M. Jimenez-Andrade, M.A. Lawson, A.M. Heegaard, Differential

pain-related behaviors and bone disease in immunocompetent mouse models of myeloma, JBMR Plus 4 (2) (2020) e10252.
[17] C.M. Peters, J.R. Ghilardi, C.P. Keyser, K. Kubota, T.H. Lindsay, N.M. Luger, D. B. Mach, M.J. Schwei, M.A. Sevcik, P.W. Mantyh, Tumor-induced injury of primary afferent sensory nerve fibers in bone cancer pain, Exp. Neurol. 193 (1) (2005) 85–100.
[18] S.A. Grenald, T.M. Doyle, H. Zhang, L.M. Slosky, Z. Chen, T.M. Largent-Milnes, S. Spiegel, T.W. Vanderah, D. Salvemini, Targeting the S1P/S1PR1 axis mitigates cancer-induced bone pain and neuroinflammation, Pain 158 (9) (2017) 1733–1742.
[19] A.P. Bloom, J.M. Jimenez-Andrade, R.N. Taylor, G. Castaneda-Corral, M. J. Kaczmarska, K.T. Freeman, K.A. Coughlin, J.R. Ghilardi, M.A. Kuskowski, P. W. Mantyh, Breast cancer-induced bone remodeling, skeletal pain, and sprouting of sensory nerve fibers, J. Pain 12 (6) (2011) 698–711.
[20] J.R. Ghilardi, K.T. Freeman, J.M. Jimenez-Andrade, W.G. Mantyh, A.P. Bloom, M. A. Kuskowski, P.W. Mantyh, Administration of a tropomyosin receptor kinase inhibitor attenuates sarcoma-induced nerve sprouting, neuroma formation and bone cancer pain, Mol. Pain 6 (2010) 87.
[21] J.M. Jimenez-Andrade, A.P. Bloom, J.I. Stake, W.G. Mantyh, R.N. Taylor, K. T. Freeman, J.R. Ghilardi, M.A. Kuskowski, P.W. Mantyh, Pathological sprouting of adult nociceptors in chronic prostate cancer-induced bone pain, J. Neurosci. 30 (44) (2010) 14649–14656.
[22] W.G. Mantyh, J.M. Jimenez-Andrade, J.I. Stake, A.P. Bloom, M.J. Kaczmarska, R. N. Taylor, K.T. Freeman, J.R. Ghilardi, M.A. Kuskowski, P.W. Mantyh, Blockade of nerve sprouting and neuroma formation markedly attenuates the development of late stage cancer pain, Neuroscience 171 (2) (2010) 588–598.
[23] M. Diaz-delCastillo, O. Palasca, T.T. Nemler, D.M. Thygesen, N.A. Chavez-Saldana, J.A. Vazquez-Mora, L.Y. Ponce Gomez, L.J. Jensen, H. Evans, R.E. Andrews, A. Mandal, D. Neves, P. Mehlen, J.P. Caruso, P.M. Dougherty, T.J. Price, A. Chantry, M.A. Lawson, T.L. Andersen, J.M. Jimenez-Andrade, A.M. Heegaard, Metastatic infiltration of nervous tissue and periosteal nerve sprouting in multiple myeloma-induced bone pain in mice and human, J. Neurosci. 43 (29) (2023) 5414–5430.
[24] T. Okui, M. Hiasa, S. Ryumon, K. Ono, Y. Kunisada, S. Ibaragi, A. Sasaki, G. D. Roodman, F.A. White, T. Yoneda, The HMGB1/RAGE axis induces bone pain associated with colonization of 4T1 mouse breast cancer in bone, J. Bone Oncol. 26 (2021), 100330.
[25] L.M. Slosky, T.M. Largent-Milnes, T.W. Vanderah, Use of animal models in understanding cancer-induced bone pain, Cancer Growth Metastasis 8 (Suppl 1) (2015) 47–62.
[26] S.H.J. Sliepen, M. Diaz-Delcastillo, J. Korioth, R.B. Olsen, C.K. Appel, T. Christoph, A.M. Heegaard, K. Rutten, Cancer-induced bone pain impairs burrowing behaviour in mouse and rat, In Vivo 33 (4) (2019) 1125–1132.
[27] K.G. Halvorson, M.A. Sevcik, J.R. Ghilardi, T.J. Rosol, P.W. Mantyh, Similarities and differences in tumor growth, skeletal remodeling and pain in an osteolytic and osteoblastic model of bone cancer, Clin. J. Pain 22 (7) (2006) 587–600.
[28] K.G. Halvorson, K. Kubota, M.A. Sevcik, T.H. Lindsay, J.E. Sotillo, J.R. Ghilardi, T. J. Rosol, L. Boustany, D.L. Shelton, P.W. Mantyh, A blocking antibody to nerve growth factor attenuates skeletal pain induced by prostate tumor cells growing in bone, Cancer Res. 65 (20) (2005) 9426–9435.
[29] M.L. Thompson, J.M. Jimenez-Andrade, S. Chartier, J. Tsai, E.A. Burton, G. Habets, P.S. Lin, B.L. West, P.W. Mantyh, Targeting cells of the myeloid lineage attenuates pain and disease progression in a prostate model of bone cancer, Pain 156 (9) (2015) 1692–1702.
[30] T.E. King, S.C. Pawar, L. Majuta, I.C. Sroka, D. Wynn, M.C. Demetriou, R.B. Nagle, F. Porreca, A.E. Cress, The role of alpha 6 integrin in prostate cancer migration and bone pain in a novel xenograft model, PLoS One 3 (10) (2008) e3535.
[31] P.M. Grace, V.L. Tawfik, C.I. Svensson, M.D. Burton, M.L. Loggia, M.R. Hutchinson, The neuroimmunology of chronic pain: from rodents to humans, J. Neurosci. 41 (5) (2021) 855–865.
[32] L. Xiang, D.M. Gilkes, The contribution of the immune system in bone metastasis pathogenesis, Int. J. Mol. Sci. 20 (4) (2019).
[33] M. Llorian-Salvador, M. Pevida, M.T. Fernandez-Garcia, A. Lastra, A. Obaya, S. Cal, A. Hidalgo, L. Menendez, A. Baamonde, Hypernociceptive responses following the intratibial inoculation of RM1 prostate cancer cells in mice, Prostate 75 (1) (2015) 70–83.
[34] J. Xu, M.D. Zhu, X. Zhang, H. Tian, J.H. Zhang, X.B. Wu, Y.J. Gao, NFkappaB-mediated CXCL1 production in spinal cord astrocytes contributes to the maintenance of bone cancer pain in mice, J. Neuroinflammation 11 (2014) 38.
[35] Z. Liu, S.F. Murphy, J. Huang, L. Zhao, C.C. Hall, A.J. Schaeffer, E.M. Schaeffer, P. Thumbikat, A novel immunocompetent model of metastatic prostate cancer-induced bone pain, Prostate 80 (10) (2020) 782–794.
[36] P.A. Baley, K. Yoshida, W. Qian, I. Sehgal, T.C. Thompson, Progression to androgen insensitivity in a novel in vitro mouse model for prostate cancer, J. Steroid Biochem. Mol. Biol. 52 (5) (1995) 403–413.
[37] S.J. Hall, S.E. Mutchnik, S.H. Chen, S.L. Woo, T.C. Thompson, Adenovirus-mediated herpes simplex virus thymidine kinase gene and ganciclovir therapy leads to systemic activity against spontaneous and induced metastasis in an orthotopic mouse model of prostate cancer, Int. J. Cancer 70 (2) (1997) 183–187.
[38] G. McCaffrey, M.L. Thompson, L. Majuta, M.N. Fealk, S. Chartier, G. Longo, P. W. Mantyh, NGF blockade at early times during bone cancer development attenuates bone destruction and increases limb use, Cancer Res. 74 (23) (2014) 7014–7023.
[39] M.R. Eber, J.M. Jimenez-Andrade, C.M. Peters, Y. Shiozawa, A method of bone-metastatic tumor progression assessment in mice using longitudinal radiography, Methods Mol. Biol. 2413 (2022) 1–6.
[40] M.L. Bouxsein, S.K. Boyd, B.A. Christiansen, R.E. Guldberg, K.J. Jepsen, R. Muller, Guidelines for assessment of bone microstructure in rodents using micro-computed tomography, J. Bone Miner. Res. 25 (7) (2010) 1468–1486.
[41] V. Arora, T.J. Martin, C.A. Aschenbrenner, K. Hayashida, S.A. Kim, R.A. Parker, J. C. Eisenach, C.M. Peters, Psychosocial stress delays recovery of postoperative pain following incisional surgery in the rat, Neuroscience 382 (2018) 35–47.
[42] J.M. Hou, J.L. Lin, J.P. Wen, L. Jin, F.Q. Tang, Immunohistochemical identification of osteoclasts and multinucleated macrophages, Cell Immunol. 292 (1–2) (2014) 53–56.
[43] K.A. Edwards, J.J. Havelin, M.I. McIntosh, H.A. Ciccone, K. Pangilinan, I. Imbert, T.M. Largent-Milnes, T. King, T.W. Vanderah, J.M. Streicher, A kappa opioid receptor agonist blocks bone cancer pain without altering bone loss, tumor size, or cancer cell proliferation in a mouse model of cancer-induced bone pain, J. Pain 19 (6) (2018) 612–625.
[44] J.G. Guedon, G. Longo, L.A. Majuta, M.L. Thomspon, M.N. Fealk, P.W. Mantyh, Dissociation between the relief of skeletal pain behaviors and skin hypersensitivity in a model of bone cancer pain, Pain 157 (6) (2016) 1239–1247.
[45] J. Ismy, D.R. Emril, Rizkidawati, Management of cancer pain with analgetic adjuvant and weak opioid in prostate cancer bone metastases: a case series, Ann. Med. Surg. (lond) 60 (2020) 575–578.
[46] C. Ripamonti, E. Fagnoni, T. Campa, V. Giardina, C. Brunelli, A. Pigni, F. De Conno, Decreases in pain at rest and movement-related pain during zoledronic acid treatment in patients with bone metastases due to breast or prostate cancer: a pilot study, Support Care Cancer 15 (10) (2007) 1177–1184.
[47] T.E. Kahkonen, J.M. Tuomela, T.J. Gronroos, J.M. Halleen, K.K. Ivaska, P. L. Harkonen, Dovitinib dilactic acid reduces tumor growth and tumor-induced bone changes in an experimental breast cancer bone growth model, J. Bone Oncol. 16 (2019), 100232.
[48] S. Falk, C.K. Appel, H.B. Bennedbaek, T. Al-Dihaissy, A. Unger, K. Dinkel, A. M. Heegaard, Chronic high dose P2X7 receptor inhibition exacerbates cancer-induced bone pain, Eur. J. Pharmacol. 845 (2019) 48–55.
[49] R. Kandasamy, M.M. Morgan, 'Reinventing the wheel' to advance the development of pain therapeutics, Behav. Pharmacol. 32 (2&3) (2021) 142–152.
[50] A. Tappe-Theodor, T. King, M.M. Morgan, Pros and Cons of clinically relevant methods to assess pain in rodents, Neurosci. Biobehav. Rev. 100 (2019) 335–343.
[51] A.N. Lozano-Ondoua, K.E. Hanlon, A.M. Symons-Liguori, T.M. Largent-Milnes, J. J. Havelin, H.L. Ferland 3rd, A. Chandramouli, M. Owusu-Ankomah, T. Nikolich-Zugich, A.P. Bloom, J.M. Jimenez-Andrade, T. King, F. Porreca, M.A. Nelson, P. W. Mantyh, T.W. Vanderah, Disease modification of breast cancer-induced bone remodeling by cannabinoid 2 receptor agonists, J. Bone Miner. Res. 28 (1) (2013) 92–107.
[52] T. King, A. Vardanyan, L. Majuta, O. Melemedjian, R. Nagle, A.E. Cress, T. W. Vanderah, J. Lai, F. Porreca, Morphine treatment accelerates sarcoma-induced bone pain, bone loss, and spontaneous fracture in a murine model of bone cancer, Pain 132 (1–2) (2007) 154–168.
[53] N.P. McCabe, M. Madajka, A. Vasanji, T.V. Byzova, Intraosseous injection of RM1 murine prostate cancer cells promotes rapid osteolysis and periosteal bone deposition, Clin. Exp. Metastasis 25 (5) (2008) 581–590.
[54] A.C. Wu, Y. He, A. Broomfield, N.J. Paatan, B.S. Harrington, H.W. Tseng, E. A. Beaven, D.M. Kiernan, P. Swindle, A.B. Clubb, J.P. Levesque, I.G. Winkler, M. T. Ling, B. Srinivasan, J.D. Hooper, A.R. Pettit, CD169(+) macrophages mediate pathological formation of woven bone in skeletal lesions of prostate cancer, J. Pathol. 239 (2) (2016) 218–230.
[55] R.S. Rana, J.S. Wu, R.L. Eisenberg, Periosteal reaction, AJR Am. J. Roentgenol. 193 (4) (2009) W259–W272.
[56] C. Geis, M. Graulich, A. Wissmann, T. Hagenacker, J. Thomale, C. Sommer, M. Schafers, Evoked pain behavior and spinal glia activation is dependent on tumor necrosis factor receptor 1 and 2 in a mouse model of bone cancer pain, Neuroscience 169 (1) (2010) 463–474.
[57] K. Chen, Y. Jiao, L. Liu, M. Huang, C. He, W. He, J. Hou, M. Yang, X. Luo, C. Li, Communications between bone marrow macrophages and bone cells in bone remodeling, Front. Cell Dev. Biol. 8 (2020), 598263.
[58] I.N. Day, R.J. Thompson, UCHL1 (PGP 9.5): neuronal biomarker and ubiquitin system protein, Prog. Neurobiol. 90 (3) (2010) 327–362.
[59] Z. Feng, S. Tao, Z. Huang, B. Zheng, X. Kong, Y. Xiang, Q. Zhang, H. Song, Z. Xu, X. Wei, F. Zhao, J. Chen, The deubiquitinase UCHL1 negatively controls osteoclastogenesis by regulating TAZ/NFATC1 signalling, Int. J. Biol. Sci. 19 (8) (2023) 2319–2332.
[60] R.B. Hansen, M. Sayilekshmy, M.S. Sorensen, A.H. Jorgensen, I.B. Kanneworff, E.K. E. Bengtsson, T.A. Grum-Schwensen, M.M. Petersen, C. Ejersted, T.L. Andersen, C. M. Andreasen, A.M. Heegaard, Neuronal sprouting and reorganization in bone tissue infiltrated by human breast cancer cells, Front. Pain Res. (lausanne) 3 (2022), 887747.
[61] M.W. Kucharczyk, K.I. Chisholm, F. Denk, A.H. Dickenson, K. Bannister, S. B. McMahon, The impact of bone cancer on the peripheral encoding of mechanical pressure stimuli, Pain 161 (8) (2020) 1894–1905.
[62] H. Tsujino, E. Kondo, T. Fukuoka, Y. Dai, A. Tokunaga, K. Miki, K. Yonenobu, T. Ochi, K. Noguchi, Activating transcription factor 3 (ATF3) induction by axotomy in sensory and motoneurons: a novel neuronal marker of nerve injury, Mol. Cell Neurosci. 15 (2) (2000) 170–182.
[63] J.M. Braz, A.I. Basbaum, Differential ATF3 expression in dorsal root ganglion neurons reveals the profile of primary afferents engaged by diverse noxious chemical stimuli, Pain 150 (2) (2010) 290–301.
[64] T. Hokfelt, X. Zhang, Z. Wiesenfeld-Hallin, Messenger plasticity in primary sensory neurons following axotomy and its functional implications, Trends Neurosci. 17 (1) (1994) 22–30.

[65] L. Calza, M. Pozza, M. Zanni, C.U. Manzini, E. Manzini, T. Hokfelt, Peptide plasticity in primary sensory neurons and spinal cord during adjuvant-induced arthritis in the rat: an immunocytochemical and in situ hybridization study, Neuroscience 82 (2) (1998) 575–589.
[66] J. Donnerer, R. Schuligoi, C. Stein, Increased content and transport of substance P and calcitonin gene-related peptide in sensory nerves innervating inflamed tissue: evidence for a regulatory function of nerve growth factor in vivo, Neuroscience 49 (3) (1992) 693–698.
[67] S. Gutierrez, J.C. Eisenach, M.D. Boada, Seeding of breast cancer cell line (MDA-MB-231(LUC+)) to the mandible induces overexpression of substance P and CGRP throughout the trigeminal ganglion and widespread peripheral sensory neuropathy throughout all three of its divisions, Mol. Pain 17 (2021).
[68] K. Tanaka, T. Kondo, M. Narita, T. Muta, S. Yoshida, D. Sato, Y. Suda, Y. Hamada, T. Shimizu, N. Kuzumaki, M. Narita, Cancer aggravation due to persistent pain signals with the increased expression of pain-related mediators in sensory neurons of tumor-bearing mice, Mol. Brain 16 (1) (2023) 19.
[69] C. Ke, C. Li, X. Huang, F. Cao, D. Shi, W. He, H. Bu, F. Gao, T. Cai, A.O. Hinton Jr., Y. Tian, Protocadherin20 promotes excitatory synaptogenesis in dorsal horn and contributes to bone cancer pain, Neuropharmacology 75 (2013) 181–190.
[70] Y. Liang, Y. Liu, B. Hou, W. Zhang, M. Liu, Y.E. Sun, Z. Ma, X. Gu, CREB-regulated transcription coactivator 1 enhances CREB-dependent gene expression in spinal cord to maintain the bone cancer pain in mice, Mol. Pain 12 (2016).
[71] L.R. Gardell, M. Ibrahim, R. Wang, Z. Wang, M.H. Ossipov, T.P. Malan Jr., F. Porreca, J. Lai, Mouse strains that lack spinal dynorphin upregulation after peripheral nerve injury do not develop neuropathic pain, Neuroscience 123 (1) (2004) 43–52.
[72] Z. Wang, L.R. Gardell, M.H. Ossipov, T.W. Vanderah, M.B. Brennan, U. Hochgeschwender, V.J. Hruby, T.P. Malan Jr., J. Lai, F. Porreca, Pronociceptive actions of dynorphin maintain chronic neuropathic pain, J. Neurosci. 21 (5) (2001) 1779–1786.
[73] Z.Y. Zhuang, P. Gerner, C.J. Woolf, R.R. Ji, ERK is sequentially activated in neurons, microglia, and astrocytes by spinal nerve ligation and contributes to mechanical allodynia in this neuropathic pain model, Pain 114 (1–2) (2005) 149–159.
[74] L.N. Wang, M. Yao, J.P. Yang, J. Peng, Y. Peng, C.F. Li, Y.B. Zhang, F.H. Ji, H. Cheng, Q.N. Xu, X.Y. Wang, J.L. Zuo, Cancer-induced bone pain sequentially activates the ERK/MAPK pathway in different cell types in the rat spinal cord, Mol. Pain 7 (2011) 48.
[75] M. Diaz-delCastillo, R.B. Hansen, C.K. Appel, L. Nielsen, S.N. Nielsen, K. Karyniotakis, L.M. Dahl, R.B. Andreasen, A.M. Heegaard, Modulation of rat cancer-induced bone pain is independent of spinal microglia activity, Cancers (basel) 12 (10) (2020).
[76] A. Hald, S. Nedergaard, R.R. Hansen, M. Ding, A.M. Heegaard, Differential activation of spinal cord glial cells in murine models of neuropathic and cancer pain, Eur. J. Pain 13 (2) (2009) 138–145.
[77] J.P. Vit, P.T. Ohara, D.A. Tien, J.R. Fike, L. Eikmeier, A. Beitz, G.L. Wilcox, L. Jasmin, The analgesic effect of low dose focal irradiation in a mouse model of bone cancer is associated with spinal changes in neuro-mediators of nociception, Pain 120 (1–2) (2006) 188–201.
[78] K.G. Halvorson, M.A. Sevcik, J.R. Ghilardi, L.J. Sullivan, N.J. Koewler, F. Bauss, P. W. Mantyh, Intravenous ibandronate rapidly reduces pain, neurochemical indices of central sensitization, tumor burden, and skeletal destruction in a mouse model of bone cancer, J. Pain Symptom Manage 36 (3) (2008) 289–303.
[79] J.B. Pineda-Farias, J.L. Saloman, N.N. Scheff, Animal models of cancer-related pain: current perspectives in translation, Front. Pharmacol. 11 (2020), 610894.
[80] J.E. Talmadge, R.K. Singh, I.J. Fidler, A. Raz, Murine models to evaluate novel and conventional therapeutic strategies for cancer, Am. J. Pathol. 170 (3) (2007) 793–804.
[81] R.R. Hansen, C.K. Nielsen, A. Nasser, S.I.M. Thomsen, L.F. Eghorn, Y. Pham, C. Schulenburg, S. Syberg, M. Ding, S.S. Stojilkovic, N.R. Jorgensen, A. M. Heegaard, P2X7 receptor-deficient mice are susceptible to bone cancer pain, Pain 152 (8) (2011) 1766–1776.
[82] D. Huang, X.L. Huang, X.B. Yan, L.X. Wu, M.A. Wang, Establishment and evaluation of a bone cancer pain model, Zhong Nan Da Xue Xue Bao Yi Xue Ban 33 (2) (2008) 115–120.
[83] C.M. Peters, E. Munoz-Islas, M.B. Ramirez-Rosas, J.M. Jimenez-Andrade, Mechanisms underlying non-malignant skeletal pain, Current Opinion in Physiology (11) (2019) 103-8.